Tellus (2005), 57A, 357–374
Printed in UK. All rights reserved

TELLUS

Impact of atmospheric horizontal resolution on El Niño Southern Oscillation forecasts

By SILVIO GUALDI*, ANDREA ALESSANDRI and ANTONIO NAVARRA, *Dynamical Climatology Group, National Institute of Geophysics and Volcanology, v. D. Creti 12, 40128 Bologna, Italy*

(Manuscript received 16 April 2004; in final form 21 October 2004)

ABSTRACT

In this paper, we assess the skill of a seasonal forecast system to predict El Niño Southern Oscillation (ENSO) anomalies and the impact that the horizontal resolution of the atmospheric component has on the forecasts of the growing phase of strong ENSO events.

The analysis has been carried out on retrospective six-month forecasts for the period 1973–2001 performed with the Istituto Nazionale di Geofisica e Vulcanologia (INGV) coupled ocean–atmosphere general circulation model (SINTEX) in the framework of the DEMETER project. Each forecast is formed by an ensemble of nine integrations that start from perturbed initial conditions. In order to consider the possible impact of the seasonal cycle on the forecasts, four different dates of the year have been chosen as initial conditions.

The results indicate that, in general, the model is reasonably good in predicting the distribution of the seasonal anomalies in the tropical Pacific. However, it is also shown that the model predictions underestimate substantially the amplitude of the anomalies during the developing phase of intense El Niño episodes.

The forecasts of strong ENSO events in the period here considered have been repeated, increasing the horizontal resolution of the atmospheric component. In these experiments, both the ocean model component and the oceanic initial conditions are unchanged. During the decaying phase of the oscillation, the high-resolution and low-resolution versions of the model produce similar results and the forecasts are in general good agreement with the observations. During the developing phase of ENSO, the low-resolution version of the model is unable to sustain the growth of the coupled disturbance. With the low-resolution atmosphere, the initial perturbation of the coupled system decays and the anomalies in the tropical Pacific tend to vanish very quickly. With the high-resolution atmosphere, on the other hand, the model appears to be able to sustain the growth of the disturbance, improving the quality of the forecasts both for El Niño and La Niña cases.

1. Introduction

The variability of climate conditions from seasonal to interannual time-scales has an enormous impact on human activity. Crop yield results, water reservoir and energy demand management are only a few examples of the environmental parameters that are strongly influenced by climate variations at these time-scales. Therefore, reliable seasonal forecasts are of great value and large public interest.

The strongest signal on the short-range climatic time-scale (from a few months to several years) is the El Niño Southern Oscillation (ENSO). Although ENSO originates and develops mainly in the tropical Pacific, its impacts are felt worldwide through a disruption of the atmospheric general circulation patterns (Ropelewski and Halpert, 1987); for a comprehensive review of ENSO, see also Philander (1990), and the 1998 *Journal of Geophysical Research* volume 103, special issue on the tropical ocean–global atmosphere (TOGA) decade. Severe droughts, for instance, are observed in north-west Australia and south-east Asia during an El Niño event. The north-east of Brazil and Zimbabwe are other regions where rainfall variations are highly correlated with the ENSO indices. Off the Peruvian coast, the marine ecosystem is directly affected by variations in oceanic upwelling, which have a substantial impact on the fishery industry.

Therefore, successful ENSO forecasts would offer decision makers an opportunity to take into account anticipated climate anomalies, reducing the social and economical impacts of this natural phenomenon. For these reasons, ENSO prediction studies have become a prominent field of research.

In the tropics, the atmosphere responds to a sea surface temperature (SST) distribution in a coherent and reproducible way (Stern and Miyakoda, 1995). Therefore, forecasting at seasonal time-scale is linked to the availability of accurately predicted SST. The dynamics of the ocean has the same fundamental

*Corresponding author.
e-mail: gualdi@bo.ingv.it

non-linearities of the atmosphere, and so it will exhibit a similar sensitivity to initial conditions. However, because the characteristic time-scales of the ocean are longer, the predictability limit will be correspondingly longer, for example several seasons. Predictions at this range therefore become a matter of predicting the SST, resulting in an atmospheric boundary problem and in an oceanic initial value problem.

In the past, a large variety of both statistical and physical ENSO prediction models have been developed and applied (Latif et al., 1998). Some notable prediction skill has been achieved with both statistical, intermediate and hybrid models. However, nowadays most of the major meteorological centres around the world produce dynamical seasonal forecasts with comprehensive ocean–atmosphere coupled general circulation models (CGCMs), using the ensemble approach (e.g. Mason et al., 1999; Kanamitsu et al., 2002).

The advantage of CGCMs relative to statistical approaches is that most of the tunable parameters have strong physical constrains. In CGCMs, parameters are not tuned for best prediction skill but to give the best representation of the physical laws. Also, simplified anomaly models were instrumental in clarifying basic ENSO dynamics. Nevertheless, they omit important processes. For instance, their assessment of off-equator processes and more remote effects is still incomplete (Perigaud et al., 2000).

An important issue in carrying out an ENSO forecast is the initialization of the forecast system. In particular, because the memory of the system resides in the upper ocean, it is crucial to determine the oceanic initial state as accurately as possible. Usually, the ocean initial conditions for an ENSO forecast system are produced with an uncoupled integration of the ocean, forcing the ocean model with observed wind stresses, heat and fresh water fluxes. Errors in the initial state are thus mainly due to model errors or to errors in the forcing. Several recent studies have shown that data assimilation techniques may help to compensate for these errors during the initialization phase (e.g. Fischer, 2002).

A successful initialization of the forecast system does not, however, guarantee successful ENSO predictions. A major source of errors for dynamical ENSO forecasts performed with CGCMs are the systematic errors that most of the models exhibit. Systematic errors can, in fact, have a strong impact on the ocean–atmosphere coupling, which, in turn, leads to severe errors in the forecasts.

Further problems can be induced by higher-order statistics. Most of the coupled models clearly underestimate the variability associated with ENSO activity (e.g. AchutaRao and Sperber, 2002). In particular, the model ENSO anomalies of SST and upper ocean heat content (HC) are generally much smaller than observed. Also, the lag autocorrelations of the model SST anomalies in the tropical Pacific tend to be smaller than observed, indicating that, in general, CGCMs have problems with both the amplitude and the phase of the ENSO cycle.

Thus, even when the initialization procedure of an ENSO forecast system is successful, producing oceanic initial states very close to the observed ones, the coupled model might be out of balance when those realistic oceanic initial conditions are used. As pointed out by Schneider et al. (2003), this initial out of balance induces an initial shock in the coupled system, which, in turn, can be transmitted to remote locations by both atmospheric and oceanic waves, degrading the forecasts.

Schneider et al. (2003) show also evidence that the initial shock tends to be more severe for January than July initial conditions. The adjustments of the models to their weak variability induce forecast errors, which tend to be more pronounced during boreal spring. This suggests that the so-called 'spring predictability barrier' (e.g. Webster, 1995) is associated with a 'spring variability barrier' (Schneider et al., 2003).

Most present-day CGCMs claim an ENSO-like variability. However, coupled models display a wide variety of behaviour and concomitant skill (e.g. Davey et al., 2001; AchutaRao and Sperber, 2002). Schneider et al. (2003) compared the ENSO forecasts performed with a set of coupled models using the same ocean model and oceanic initial conditions, but different atmospheric components. Their findings indicate that the systematic errors of the coupled predictions are large and depend on the season and on the atmosphere model. They also investigated the sensitivity of the ENSO forecasts to the horizontal resolution of the ocean model, finding that the skill in predicting ENSO anomalies is basically independent of the oceanic resolution.

Guilyardi et al. (2004) have used a systematic modular approach to investigate the respective roles of the ocean and atmosphere in setting ENSO characteristics in an ensemble of CGCMs. Their results, in agreement with Schneider et al. (2003), show a dominant role of the atmosphere model in determining some of the main characteristics and errors of the simulated ENSO. Furthermore, analyses of the impact of the atmospheric component resolution on the simulation of ENSO have shown a considerable improvement of the simulated oscillation when the atmosphere resolution is significantly increased (Gualdi et al., 2003a; Guilyardi et al., 2004). A possible explanation for the positive impact of the increased atmospheric resolution might be related to a better capture of the details of the modelled SST structures, which improves the ocean–atmosphere coupling, reducing the model errors.

All these results indicate that a reduction of the model errors has a large potential for improving the forecast skill. In particular, the effects of the atmospheric increased resolution, which seem to have a beneficial impact on ENSO simulations (Gualdi et al., 2003a; Guilyardi et al., 2004), might be important also for the forecast of the oscillation, leading to an improvement of the forecast performance.

The main objective of this work is to investigate the sensitivity of the ENSO predictions produced with a CGCM to the horizontal resolution of the atmospheric component. The ENSO forecasts produced with the Istituto Nazionale di Geofisica e

Vulcanologia (INGV) coupled model in the framework of the DEMETER European Union (EU) project will be used to assess the skill of the system. Then, it will be shown that the capability of the system in predicting the development of intense ENSO episodes is substantially improved when a high-resolution version of the atmospheric model component is used.

In Section 2, we briefly describe the INGV seasonal forecast system as well as the data method used to validate the forecasts. The results obtained with the forecast system in its standard version are shown and discussed in Section 3. Section 4 contains the comparison between the ENSO predictions obtained with the coupled model implemented at low and high resolutions. In Section 5 we conclude the paper with a summary of the main results obtained with this work and the main conclusion we can drawn from them.

2. Forecasting system and data used in the study

The modelling data employed in this work are the seasonal predictions produced with the INGV forecast system in the framework of the EU project DEMETER. The DEMETER system is a multi-model ensemble-based system for seasonal to interannual forecasts, which comprises seven CGCMs. A complete and detailed description of DEMETER, its objectives and some discussion of its main results can be found in Palmer et al. (2004), Hagedorn et al. (2005) and Doblas-Reyes et al. (2005).

2.1. *The INGV coupled model*

The numerical model used to produce the INGV seasonal forecasts is an ocean–atmosphere CGCM developed within the Scale INTeraction EXperiment (SINTEX) EU project. The SINTEX model is formed by ECHAM-4 as atmosphere component and ORCA as ocean component. ORCA is the global version of the OPA 8.1 ocean modelling system developed by the Laboratoire d'Océanographie Dynamique et de Climatologie (LODYC) team in Paris (Madec et al., 1998; see full documentation at http://www.lodyc.jussieu.fr/opa/). It is a finite difference oceanic GCM and solves the primitive equations with a non-linear equation of state on an Arakawa C-grid. The present configuration uses a rigid lid. The horizontal mesh is orthogonal and curvilinear on the sphere, and its space resolution is roughly equivalent to a geographical mesh of $2^\circ \times 1.5^\circ$ (with a meridional resolution of 0.5° near the equator). 31 vertical levels are used with 10 levels in the top 100 m. There is no interactive sea-ice model in the configuration used for the seasonal forecasts: sea-ice cover is relaxed towards observed monthly climatology.

ECHAM-4 is the fourth generation of the ECHAM atmospheric general circulation model developed at the Max-Planck-Institut Für Meteorologie in Hamburg. The model equations are solved on 19 hybrid vertical levels (top at 10 hPa) by using the spectral transform method. In these simulations, ECHAM-4 is used with a triangular truncation T42, which corresponds to an associated Gaussian grid of approximately $2.8^\circ \times 2.8^\circ$ in latitude and longitude. A few forecasts were however performed with an higher version of the atmospheric component. In these high-resolution forecasts, the ocean component and the oceanic initial conditions are exactly the same as for the low-resolution forecasts, but the atmospheric model is used with a triangular truncation T106, corresponding to an associated Gaussian grid of approximately $1.1^\circ \times 1.1^\circ$. An exhaustive and detailed description of the dynamical and physical structure, and the simulated climatology of ECHAM-4 has been given by Roeckner et al. (1996).

The atmospheric and oceanic components were coupled through OASIS2.4 (Valcke et al., 2000). No flux adjustment or restoring were used in the simulations. Air–sea fluxes and SST were exchanged between the model components every 3 h.

The main features of the climatology simulated by the SINTEX model have been investigated in Gualdi et al. (2003a). In this study, the impacts of the atmospheric horizontal resolution on the simulated mean state and climate variability have also been assessed. The results show that, at all model resolutions, the mean SST errors relative to observations are smaller than 1°C. Differences larger than 2°C are found only in the equatorial upwelling regions (e.g. off the Peruvian coast) and along the western boundary currents in the extratropical Pacific and Atlantic.

The ocean thermal structure is reasonably realistic for all model resolutions. In the equatorial Pacific, the thermocline slope and structure, of importance for ENSO dynamics, are generally well reproduced. However, the equatorial cold tongue penetrates too far into the west Pacific due to stronger-than-observed trade winds. These intensified trades are associated to the atmospheric model (ECHAM-4) tendency to overemphasize the Walker-type circulation in the equatorial plane (Roeckner et al., 1996).

The simulated seasonal variation exhibits some problem in the eastern equatorial Pacific. Here, at all resolutions, the annual cycle of the SST appears to be underestimated compared to the observations; whereas, the seasonal and semi-annual modulation are overestimated in the central Pacific.

For a complete description and discussion of the model performance, the reader is referred to Gualdi et al. (2003a,b), Guilyardi et al. (2003) and Corti et al. (2003). In summary, the results shown and discussed in these papers indicate that the SINTEX model simulates a reasonably realistic mean state and climate variability. Furthermore, both the simulated mean state and interannual variability are generally improved when the horizontal resolution of the atmospheric model component is increased.

2.2. *Initialization procedure and forecast production*

The coupled model has been used to produce retrospective seasonal forecasts for the period 1973–2001. In order to consider the possible impact of the seasonal cycle on the forecasts, the simulations were performed starting from four different dates of the year: 1 February, 1 May, 1 August and 1 November.

The initial conditions of the ocean–atmosphere system for each starting date were obtained from separate integrations of the ocean and atmosphere model components in forced mode.

Atmospheric initial conditions were obtained from an AMIP-type run performed with the atmosphere component of the model forced with observed SSTs (HadISST1.1 Global Sea-ice and SST; Rayner et al., 2000) for the period 1972–2001.

In order to represent the uncertainties in the initial state of the ocean, an ensemble of nine ocean initial conditions has been produced. Specifically, the ocean model, ORCA, was first integrated for a 30-yr (1972–2001) control run, where the ocean was forced with momentum, heat and mass flux data from the European Centre for Medium-Range Weather Forecasts (ECMWF) 40-yr reanalysis (ERA-40; more information about the ERA-40 global analysis is available at http://www.ecmwf.int/research/era). Then, two perturbed ocean simulations, for the same period, have been performed adding daily wind stress perturbations to the ERA-40 momentum fluxes. The wind stress perturbations were taken randomly from a set of monthly differences between two quasi-independent analyses. Furthermore, in order to represent the uncertainty in SSTs, four SST perturbations were added at the initial conditions of the hindcasts. As for the wind perturbations, the SST perturbations are constructed to represent differences between two quasi-independent SST observational data sets.

In order to keep the simulated SSTs close to the observed fields, during the forced ocean integrations, the model SSTs were relaxed towards the observed SSTs (Reynolds and Smith, 1994).

In summary, for each starting date, each year of the period 1973–2001, one atmospheric initial condition and an ensemble of nine oceanic initial conditions were created. Starting from these initial conditions, the coupled model has been integrated for six months, producing sets of nine-member ensemble forecasts.

2.3. Reference data and verification methods

The predictive skill of the model is assessed comparing the retrospective forecasts with analyses and observational products. The ERA-40 reanalyses and the ocean analysis described in Masina et al. (2001) are used for verification of the forecasts. For precipitation, we use the Climate Prediction Center (CPC) Merged Analysis of Precipitation (Xie and Arkin, 1997), covering the period 1979–2001.

The model and the observed (analysis) anomalies are defined as the deviation from the model and the observed climatology, respectively. In particular, the anomalies are computed relative to the 1973–2001 simulated and observed mean state, except for the precipitation anomalies, which are calculated relative to the 1979–2001 period.

The forecast skill of the system is measured by computing the correlations of the observed and forecast anomalies. Root mean square errors (RMSEs) are also used to assess the performance of the forecasts. ENSO anomaly composites are constructed from intense El Niño and La Niña episodes, such as those that occurred during winter 1982–1983, 1987, 1997–1998 and 1984–1985, 1988–1989, 1999–2000 respectively. The composites obtained from the observations and from the forecasts are then used to estimate the capability of the system to predict strong ENSO events, and to assess the impact of the atmospheric horizontal resolution.

3. Seasonal forecasts

In this section, we present a concise description and discussion of the skill of the INGV coupled model retrospective forecasts. In particular, we focus on the capability of the system to predict the seasonal anomalies in the tropical Pacific region. For a more comprehensive and detailed analysis of the INGV forecast system skill and a comparison with the results obtained with similar systems, the reader is referred to the DEMETER web site, http://www.ecmwf.int/research/demeter.

3.1. Main features of the model bias

As already pointed out, a very important source of forecast errors with CGCMs is the systematic errors of the model. This problem is especially important for the prediction of the SST anomalies. The amplitude of the model SST bias, in fact, can be as large as the amplitude of the observed SST anomalies that should be predicted. On the other hand, a successful prediction of the SST is crucial for the skill of the seasonal forecast. Therefore, before analysing the details of the forecasts, it is of interest to show and discuss briefly the main features of the model systematic errors, focusing in particular on the SST errors in the tropical Pacific.

Figure 1 shows the SST model systematic errors for the different start dates and averaged over different forecast periods. Here, the systematic error is defined as the difference between the climatologies obtained from the forecast ensembles and from the ERA-40.

The results shown in Fig. 1 indicate that, for all start dates, the systematic error of the model in predicting the SST field is moderate in most of the tropics. Over a large portion of the tropical belt, in fact, the model exhibits an averaged cold bias smaller than 1°C. The error is remarkably small in the tropical Indian Ocean. In the south-eastern tropical Pacific and in the upwelling regions off the American coast and in the Gulf of Guinea, the model is too warm, and the averaged error is larger than 1°C.

The equatorial cold tongue is too pronounced and penetrates too far into the west Pacific, producing SST patterns too symmetrical around the equator. The results shown in Fig. 1 are consistent with the results obtained from long climate simulations performed with the coupled model (e.g. Gualdi et al., 2003a), where the tendency to produce a double intertropical

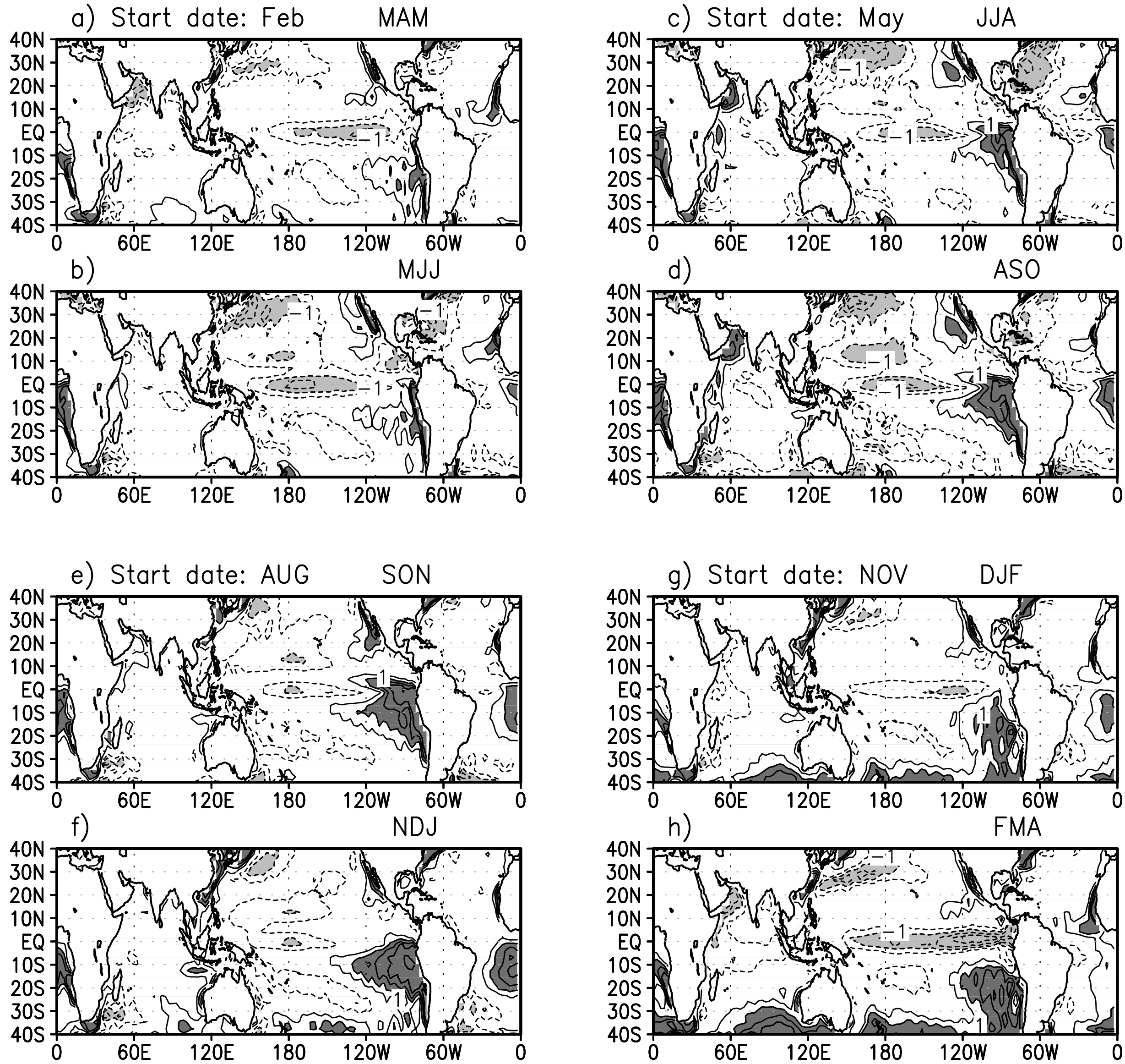

Fig 1. Model systematic error of SST. The error is defined as the difference between the climatology obtained from the forecast ensembles and the climatology obtained from the ERA-40 SSTs. (a), (b) The 2–4 month (March–May) and 4–6 month (May–July) averages of the systematic error obtained from the forecasts with start date 1 February. (c), (d) The 2–4 month (June–August) and 4–6 month (August–October) averages of the systematic error obtained from the forecasts with start date 1 May. (e), (f) The 2–4 month (September–November) and 4–6 month (November–January) averages of the systematic error obtained from the forecasts with start date 1 August. (g), (h) The 2–4 month (December–February) and 4–6 month (February–April) averages of the systematic error obtained from the forecasts with start date 1 November. Contours: solid lines correspond to positive values and dashed lines correspond to negative values. Contour interval is 0.5°C. Light shaded values correspond to negative anomalies with amplitude larger than −1°C. Dark shaded values correspond to positive anomalies with amplitude larger than 1°C.

convergence zone (ITCZ) in the tropical Pacific was documented. The double ITCZ systematic error is also visible in the model precipitation bias (not shown).

The systematic errors show also some dependency on the date of the initial conditions. For example, the SST warm bias in the tropical eastern Pacific seems to be more pronounced for the forecasts with start date in May (Figs. 1c and d) and August (Figs. 1e and f). The error in the equatorial Pacific cold tongue, on the other hand, is more evident for the forecasts starting in February (Figs. 1a and b) and November (Figs. 1g and h). In the latter case, the cold tongue bias appears to increase rather markedly during the last period of the forecast.

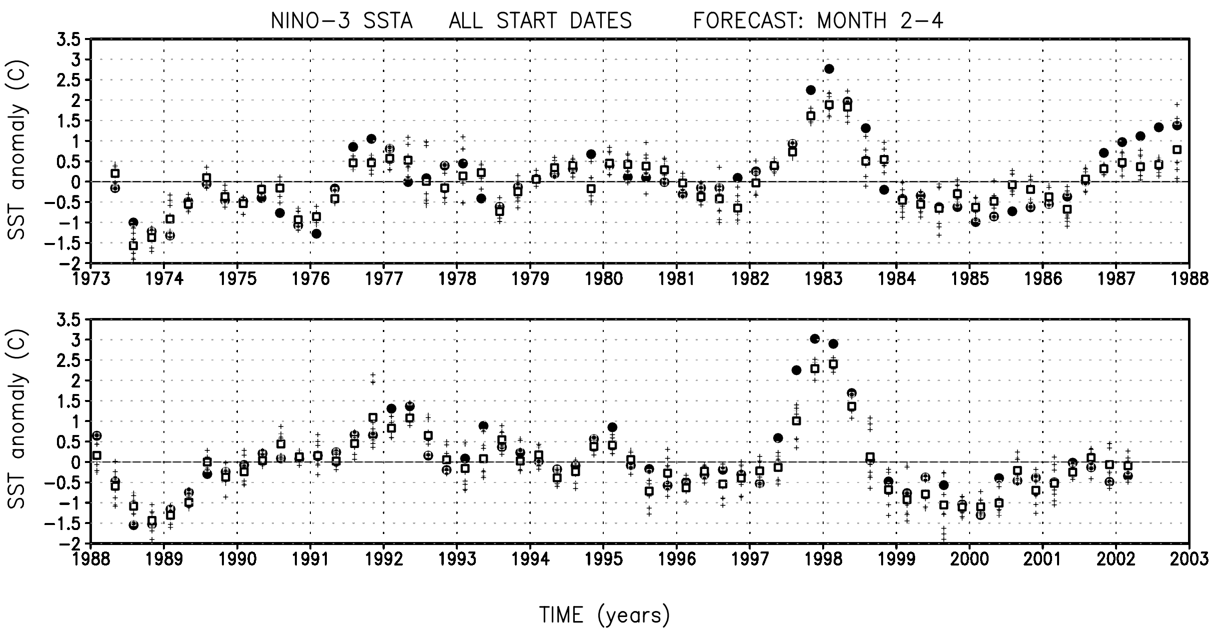

Fig 2. Time series of the SST anomaly averaged over the NINO-3 (5°S–5°N, 150°W–90°W) region. The values plotted are the 2–4 month forecast average for all start dates. The filled circles are the values obtained from the observations; the squares are the ensemble mean forecasts; the crosses are the ensemble member forecasts. The unit of the ordinate axis is °C, whereas along the abscissa are the forecast years.

3.2. Seasonal forecasts of the tropical Pacific anomalies

A first assessment of the ENSO forecasts can be given by considering the time series of the so-called NINO-3 index, which is defined as the average of the SST anomaly (SSTA) over the NINO-3 region (5°S–5°N, 150°W–90°W).

Figure 2 shows the time series of the NINO-3 months 2–4 average values, for all start dates. In other words, the NINO-3 SST values plotted in Fig. 2 are the averages over the two to four months of the anomalies predicted from all start dates. The correlation between the observed NINO-3 index (filled circles) and the predicted index as obtained from the ensemble mean forecasts (squares) is 0.90. This indicates that in most years considered, the one-month lead time forecasts capture well the amplitude of the SSTA in the NINO-3 region. With a few exceptions, the difference between the observed anomaly and the forecast ensemble mean anomaly is generally smaller than 0.5°C.

However, it is noteworthy that the discrepancy between observations and forecasts tends to be more pronounced during strong Niño events (winter 1982–1983, 1987 and winter 1997–1998). During these periods, in fact, the differences between forecasts and observations can be larger than 1°C, especially in the developing phase of the positive SST anomalies.

Although the NINO-3 index shown in Fig. 2 is frequently used to characterize the state of the ENSO and to quantify the quality of simulations and predictions of the oscillation, it describes the SSTA over only a small portion of the Pacific ocean. The oceanic anomalies associated with ENSO, on the other hand, affect the whole tropical basin. It is therefore of interest to check the skill of the forecasting system to predict the evolution of the SST anomalies over the entire tropical Pacific. To this aim, anomaly correlations and RMSEs for the forecast SSTA in the tropical Pacific (defined as 26°S–26°N, 120°E–90°W) have been computed.

Figures 3 and 4 show the anomaly correlations and the RMSEs for the forecast SSTA in the tropical Pacific, together with the results obtained for persistence forecasts. The anomaly correlations and the RMSEs have been computed relative to the ERA-40 SST. Persistence forecasts are made by persisting the observed (ERA-40) monthly anomaly from the month prior to the start date of the model forecasts. For example, SST persistence forecasts for the period February–July 1987 have been made by persisting the SSTA found for the observed January 1987.

The results shown in Figs. 3 and 4 indicate that the ensemble mean forecasts (thick solid lines) have better skill than any ensemble member (thin solid lines). This is in agreement with the results found with other coupled model forecast systems, and can be explained by the fact that the ensemble average reduces the noise present in the individual forecasts, increasing the correlations and reducing the RMSE. The ensemble mean forecasts (hereafter, simply ‘forecasts’) appear to perform generally better also than persistence forecasts (dashed lines; hereafter ‘persistence’), especially on lead times greater than two to three months.

Furthermore, both the anomaly correlations and the RMSEs show some seasonal dependence, with some suggestion

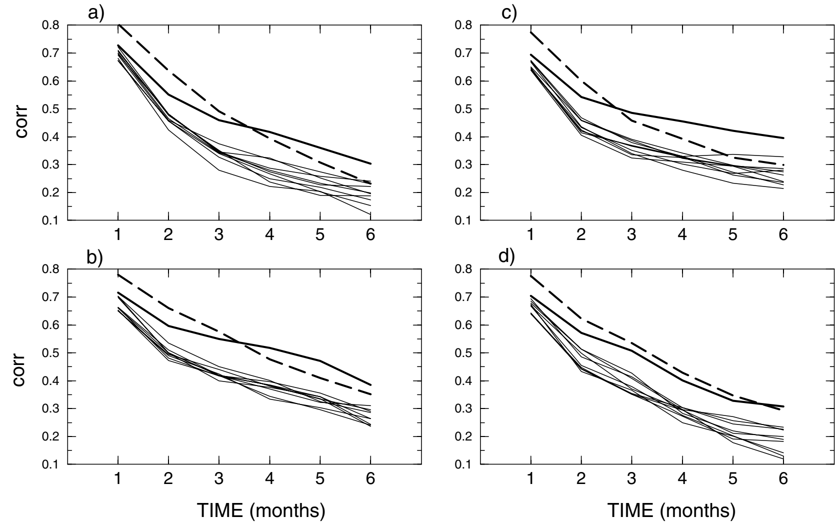

Fig 3. ACCs between predicted and observed SST anomaly distribution over the tropical Pacific (26°S–26°N, 120°E–90°W). The ACCs have been averaged over the period 1973–2001 and are plotted as a function of the forecast month (*x*-axis). (a)–(d) Forecasts with start date 1 February, 1 May, 1 August and 1 November, respectively. The solid thin lines show ensemble member forecasts, the solid thick line shows the ensemble mean forecast and the dashed thick line shows the persistence forecast. Persistence forecast is defined as the persisting monthly anomaly observed during the month prior to the start date of the model forecasts.

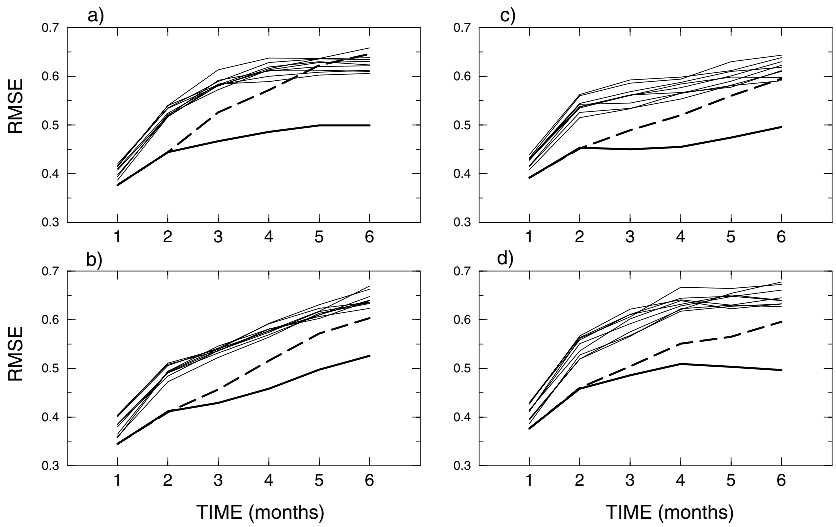

Fig 4. As Fig. 3, but for the RMSE between the predicted and the observed SST anomaly over the tropical Pacific.

of a (weak) 'spring prediction barrier'. Higher skills, in fact, are found for the forecasts that start in May and especially in August compared to the forecasts that start during northern winter (February and November). These results are consistent with Schneider et al. (2003).

The time series of the correlation coefficients and the RMSEs between forecast and ERA-40 SST anomalies, over the tropical Pacific, for the period 1973–2001 (not shown), give further evidence of the skill of the system. The correlations are generally higher than 0.6 and the model skill better than persistence. During years of intense ENSO episodes, such as 1982, 1987 and 1997, the correlations are larger than 0.9 for month 2–4 average and 0.7 for month 4–6 average forecasts. Interestingly, these are also the years for which the RMSE is largest.

These results, along with the results obtained from the DEMETER verification diagnostics (e.g. Palmer et al., 2004; see also the DEMETER web site), indicate that the skill of the forecasting system described here is comparable to the skill of the other systems based on present leading CGCMs, and that they perform at levels comparable to dedicated ENSO prediction models.

The concomitance between high correlations and large RMSEs between forecast and observed SSTA in the tropical Pacific, during intense El Niño years, suggest that the model reproduces successfully the evolution of the SSTA patterns in this region, but it has problems with the amplitude of the anomalies. This is consistent with the NINO-3 SSTA time series (Fig. 2), where it was shown how the forecasts tend to underestimate the SSTA amplitude during strong ENSO events.

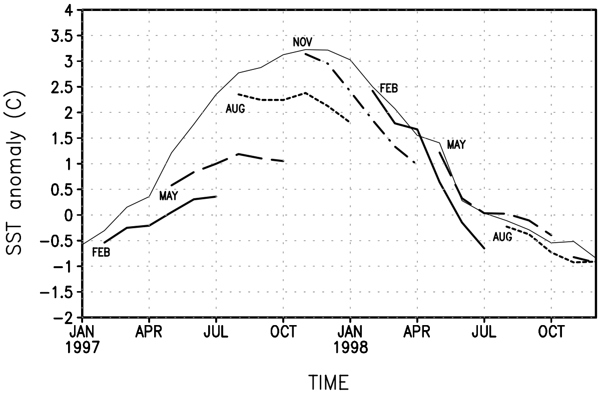

Fig 5. Time series of the NINO-3 SST anomaly for the period January 1997–December 1998: thin solid line, observations; thick solid lines, forecast with start date 1 February; thick dashed lines, forecast start date 1 May; thick dotted line, forecast with start date 1 August; thick dash-dotted line, forecast with start date 1 November.

The tendency to simulate weak ENSO anomalies is a feature common to many CGCMs (e.g. AchutaRao and Sperber, 2002; Fischer, 2002). As suggested from the results shown in Fig. 2, this problem becomes particularly evident during the developing phase of strong El Niño episodes. Figure 5, for example, shows the evolution of the NINO-3 SSTA from January 1997 to December 1998 for the ERA-40 (thin solid line) together with the forecasts for the different start dates.

During the first half of 1997, the observed SSTA increases by about 3°C in a few months. The forecasts have problems in reproducing the growing phase of the anomalies during 1997. In particular, the forecasts with February and May start dates (Fig. 5, thick solid and dashed lines) systematically underestimate the amplitude of the developing anomalies. On the other hand, the forecasts with August and November start dates (Fig. 5, thick dotted and dash-dotted lines) clearly tend to bring forward the turnabout of El Niño, predicting an early decay of the SST anomalies.

It is also interesting to note that a better performance is obtained for the forecasts of the decaying phase of the 1997–1998 El Niño. Figure 5, in fact, shows that the NINO-3 SSTA predicted for the period February–December 1998 are very close to the observations, in terms of both amplitude and phase.

The results shown in Fig. 5 suggest that the model has difficulties in forecasting the development of intense ENSO episodes, such as the 1997–1998 El Niño. This suggestion is further confirmed when the evolution of upper ocean HC, SST and precipitation anomalies over the entire tropical Pacific are considered.

Figure 6 shows the HC (left column panels), SST and precipitation (right column panels) anomalies obtained from the ocean analyses and observations for the period February–July 1997. During February and March, large positive anomalies are observed in the west Pacific; whereas negative SST anomalies are located in the eastern part of the basin. Between April and May, the positive anomaly of HC propagates across the equatorial Pacific reaching the South American coast. In the following months (June and July), intense positive HC, SST and precipitation anomalies develop in the central-eastern Pacific.

The results obtained from the forecasts are shown in Fig. 7. A simple visual comparison of the fields shown in the two pictures clearly reveals the inability of the model to predict the amplitude of the anomalies that develop during the growing phase of the oscillation. During the first two months of the forecast (Fig. 7, upper panels) the model produces positive anomalies of HC and SST in the western Pacific between about 10°N and 10°S. The structure of the precipitation anomaly forecast (right panel, shaded patterns) appears to be more complex, with a negative anomaly south of the equator and positive anomaly developing to the north of the equator.

The anomaly distribution obtained from the first month of the forecast (not shown) exhibits patterns similar to those observed (not shown), suggesting that the initial conditions, at least for this particular forecast, were reasonably close to a realistic initial state. In the following months, however, the forecast signal vanishes very quickly.

Between April and May, the HC exhibits some evidence of a propagating anomaly, which moves from the western to the eastern equatorial Pacific, resembling the travelling signal observed during this period (Fig. 6). In the following months (June and July) there is also some suggestion of a positive SST anomaly in the eastern tropical Pacific, which is consistent with the developing El Niño.

The model thus exhibits some capability to reproduce the time evolution and some basic feature of the observed anomalies, in agreement with the reasonably good results we have obtained from a general basic assessment of the skill of the forecasts. However, the predictions seriously underestimate the amplitude of the anomalies in the tropical Pacific, during the developing phase of intense El Niño events, such as 1997–1998.

4. Sensitivity of the ENSO forecasts to the horizontal resolution of the atmosphere

In Gualdi et al. (2003a) and Guilyardi et al. (2004) it has been shown that an increase of the horizontal resolution of the atmospheric component of a CGCM produces improvements in the main features of the simulated ENSO variability. In this paper, we investigate whether increasing the horizontal resolution of the atmospheric component of the model leads to improvements also in the prediction of ENSO activity. In particular, we investigate if the tendency of the model to underestimate the amplitude of the ENSO anomalies might be reduced improving the horizontal resolution of the model.

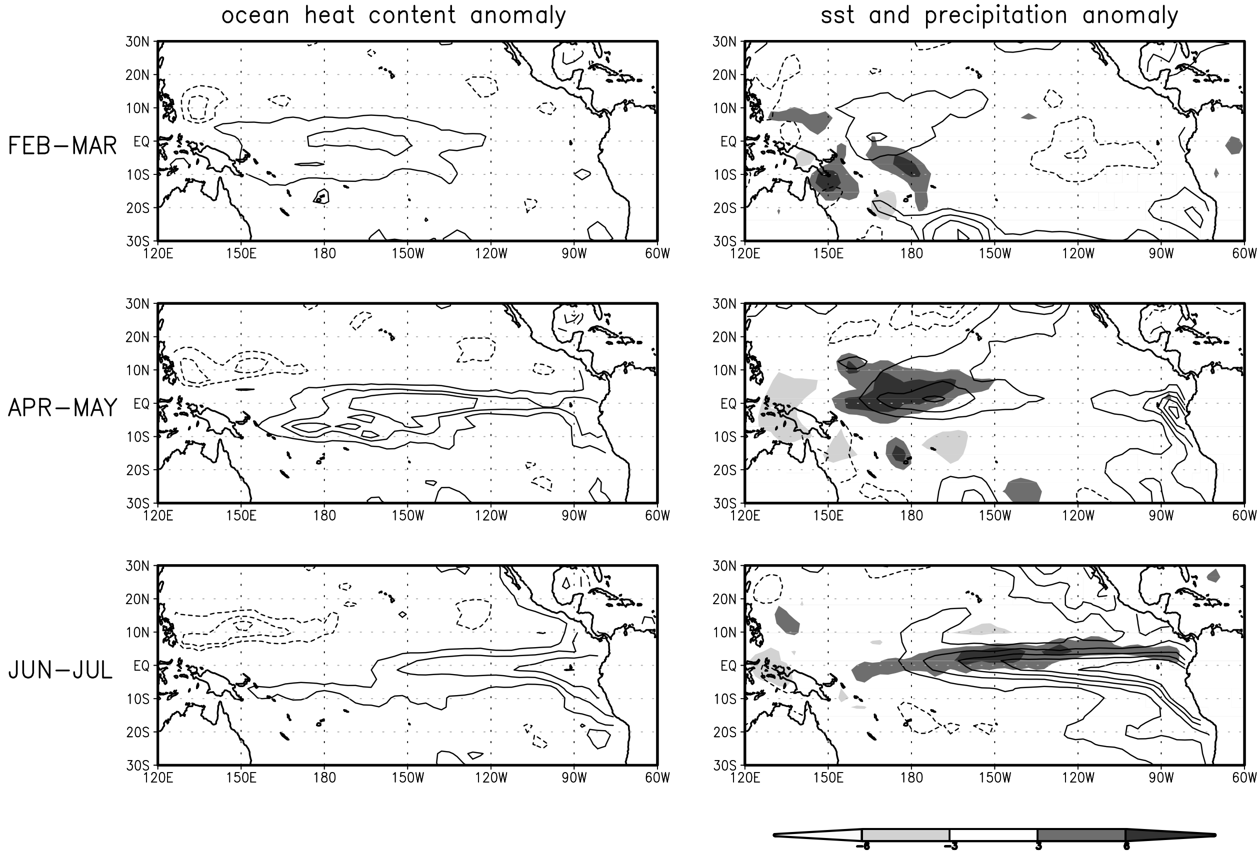

Fig 6. Evolution of the reference upper 300-m ocean HC (left panels), SST (right panels, contour patterns) and precipitation (right panels, shaded patterns) anomalies through the period February–July 1997. Contours: HC, 1×10^9 J m^{-2}; SST, 0.5°C; precipitation, 3 mm d^{-1}. Dashed contours and light shaded patterns correspond to negative values. Solid contour and dark shaded patterns correspond to positive values. The HC anomalies are obtained from an ocean analysis (Masina et al., 2001), the SST fields are from the ERA-40, and observed precipitation anomalies are from Xie and Arkin (1997).

To this aim, we have produced new sets of ensemble forecasts, increasing the horizontal resolution of the atmospheric component. Specifically, the atmospheric resolution has been increased from an approximately $2.8^\circ \times 2.8^\circ$ (T42) grid, used in the standard forecasts, to a roughly $1.1^\circ \times 1.1^\circ$ (T106) grid. All of the other components of the coupled system (ocean, coupler and oceanic initial conditions) are exactly the same as those used for the standard (low-resolution) forecasts.

Because of the very large power computing demand placed by the high-resolution version of the model, we produced the T106 forecasts only for the periods 1982–1991 and 1996–2000. Furthermore, for the same reason, only two start dates have been considered: 1 February and 1 August. Although shorter than for the T42 case, the high-resolution forecast period (15 yr) is long enough to allow some statistical assessment of the model skill. The periods 1982–1991 and 1996–2000 have been chosen to encompass the stronger ENSO events (both El Niño and La Niña) observed during the last decades.

In the following, the forecasts obtained with the high-resolution version of the model (T106) will be assessed and compared with the observations and the results obtained from the standard (T42) model forecasts. To this aim, for all of the cases (observations, T42 and T106) the anomalies are computed with respect to the mean state obtained as the average over the period 1982–1991/1996–2000. In other words, the observed anomalies, for example, have been computed as the deviation from the observed mean state obtained as the average over the period 1982–1991/1996–2000. Similarly, the T42 (T106) anomalies have been computed as the deviation from the T42 (T106) model mean state obtained as the average over the period 1982–1991/1996–2000.

Interestingly, the T42 and T106 model forecasts with initial conditions 1 August exhibit very similar features. In particular, the performance of both T42 and T106 versions of the model in predicting the decaying phase of intense ENSO events is reasonably good, as also suggested in Fig. 5. Therefore, because the differences between the T42 and T106 models during the termination of the oscillation are very small (not shown), for the sake of brevity, in the following only the forecasts of the developing phase of ENSO will be discussed.

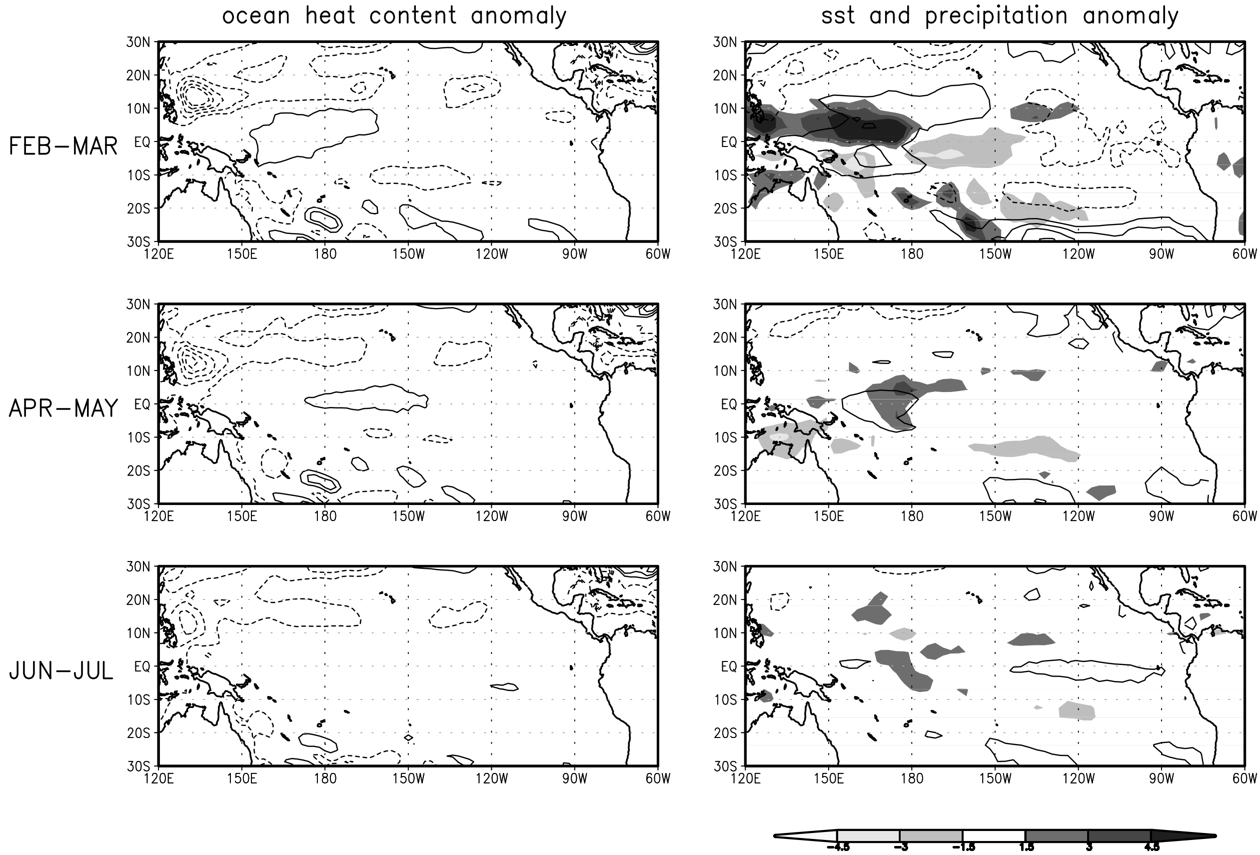

Fig 7. As Fig. 6, but for the model forecast. Contours: HC, 0.4×10^9 J m^{-2}; SST, 0.4°C; precipitation, 1.5 mm d^{-1}.

Figure 8 shows the same fields as in Figs. 6 and 7, but for the ensemble forecast experiments performed with the high-resolution atmosphere. It appears that the forecast performed with the T106 version of the atmospheric model is notably improved. In fact, not only the timing of the evolution of the simulated anomalies is realistic, but also the amplitude of the field perturbations is considerably larger than in the T42 case, and much closer to the observations.

In particular, the SST anomaly predicted with the high-resolution version of the model is substantially better. Similar to the observations, the positive anomaly of HC crosses the equatorial Pacific reaching the eastern part of the basin. Here, the SST anomaly passes from the negative values at the beginning of the forecast, to the positive values found between April and July. Associated with the warm SST anomalies, there is an increment of precipitation, which extends along the equator from the western to the central-eastern Pacific.

4.1. *Model bias with the high-resolution atmosphere*

As already pointed out, the assessment of the model systematic error is very important for the evaluation of the forecasts. Figure 9 shows the SST mean error for the T106 forecasts with start date 1 February. The bias is defined as the difference between the climatologies obtained from the T106 forecast ensembles and from the ERA-40, for the 15-yr period 1982–1991/1996–2000.

The results shown in Figs. 9, 1(a) and 1(b) indicate that the SST bias of the T106 model is similar to the T42 model systematic error, in terms of both amplitude and spatial patterns. In particular, as found for the T42 case, the T106 model exhibits a cold bias in the central-eastern equatorial Pacific. Also in this case, the equatorial cold tongue tends to penetrate too far into the west Pacific, although the amplitude of the model error appears to be reduced.

Figure 10 shows the near-surface zonal wind mean error for the T42 (left panels) and the T106 (right panels) forecasts. Consistently with the SST error, the surface wind bias shows the model tendency to overestimate the easterlies over the equatorial Pacific, for both T42 and T106 cases. However, also for the low-level zonal wind, the systematic error is reasonably small, generally smaller than 1 m s^{-1}, over most of the tropical Pacific.

More interestingly, a comparison between the T42 (Figs. 10a and b) and T106 (Figs. 10c and d) model errors reveals that the high-resolution model improves the simulation of the mean zonal wind, especially over the central and western equatorial Pacific.

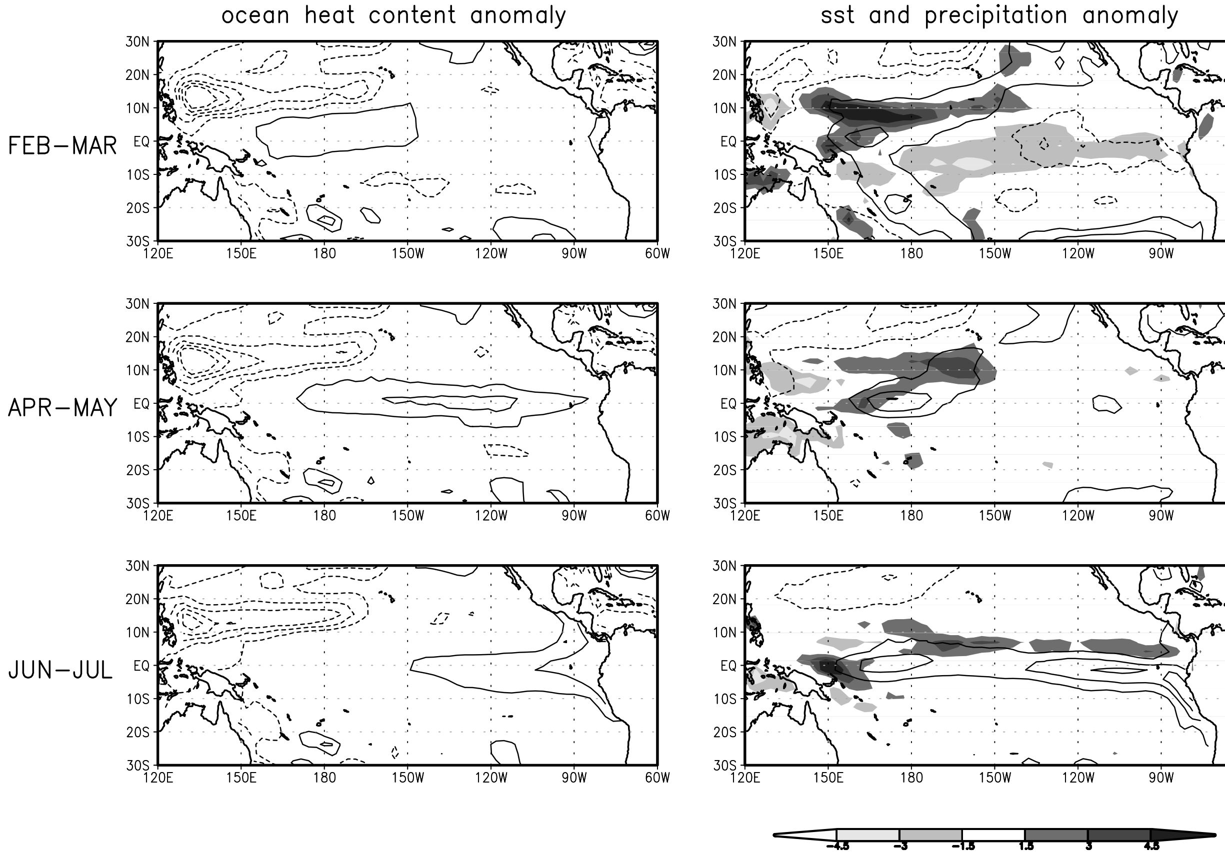

Fig 8. As Fig. 6, but for the high-resolution version (T106) of the model forecast. Contours: HC, 0.4×10^9 J m^{-2}; SST, 0.4°C; precipitation, 1.5 mm d^{-1}.

In this region, in fact, the T106 model reduces substantially the error in the surface easterlies.

The improvement of the surface winds in the equatorial Pacific leads to an improvement of the simulated ocean thermal structure in this region (not shown). In the western Pacific, the erosion of the warm pool is more pronounced in the low-resolution model; whereas, with the T106 model, both the warm pool extension and the thermocline depth are closer to the observations (not shown).

In summary, the mean error that characterizes the T106 version of the model has features similar to the bias that afflicts the T42 model, although some reduction of the error amplitude is also visible. These results are consistent with the findings of Gualdi et al. (2003), who present a detailed comparison of the climatology simulated with the coupled model implemented with different horizontal resolution of the atmosphere.

4.2. *Composites of the ENSO anomalies*

Further evidence of the impact of the increased atmospheric resolution on the ENSO anomaly forecasts is given by a composite analysis. Composites of the developing phase of El Niño anomalies have been computed by averaging the monthly anomalies for the period February–July over the years 1982, 1987 and 1997. Similarly, composites of developing La Niña anomalies have been computed by averaging the monthly anomalies for the period February–July over the years 1984, 1988 and 1999.

4.2.1. Upper ocean heat content. Figure 11 shows the composites of HC anomaly during the developing phase of El Niño, as obtained from the ocean analysis (left column panels), and as predicted with the T42 (middle column panels) and the T106 (right column panels) models.

During the first two months of the forecast (February–March, upper panels), both T42 and T106 models exhibit a positive HC anomaly that, in agreement with the ocean analysis (upper-left panel), extends from the central equatorial Pacific to the South American coast. In both cases, the HC anomaly appears to be weaker than in the analysis.

During the following months, in the ocean analysis, the maximum of the HC anomaly moves from the central to the eastern equatorial Pacific, reaching its largest amplitude between June and July. With the T42 model (middle column panels), the

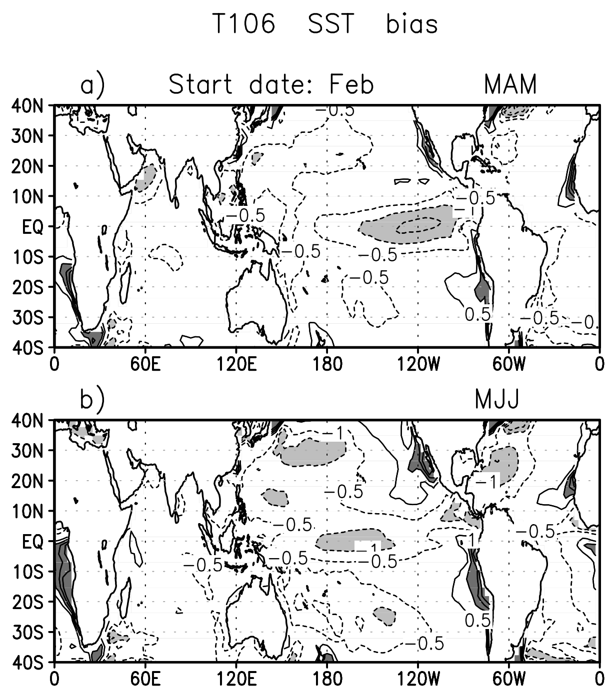

Fig 9. High-resolution model (T106) systematic error of SST. The error is defined as the difference between the climatology obtained from the forecast ensembles and the climatology obtained from the ERA-40 SSTs. For both the model and the ERA-40, the climatology have been computed as the annual mean over the period 1982–1991/1996–2000. (a), (b) The 2–4 month (March–May) and 4–6 month (May–July) averages of the SST systematic error obtained from the forecasts with start date 1 February. Contour is 0.5°C. Dark shaded values correspond to positive anomalies with amplitude larger than −1°C. Light shaded values correspond to negative anomalies with amplitude larger than 1°C.

initial disturbance decreases rapidly, and at the end of the forecasts the HC anomaly has basically vanished over the entire tropical Pacific. In the T106 forecasts, on the other hand, the evolution of the HC anomaly (right panels) is closer to the observations. The initial perturbation is sustained and its maximum, although weaker, shifts from the central to the eastern Pacific, consistent with the analysis. In the tropical western Pacific, a negative anomaly develops, in agreement with observations and with the El Niño termination mechanism discussed in Guilyardi et al. (2003).

Similar results are obtained from the composite patterns of the HC anomalies representing the developing phase of La Niña events (not shown). The ocean analysis exhibits negative anomalies that develop across the equatorial central-eastern Pacific, reaching the maximum amplitude in the eastern Pacific at the end of the forecast period (July). As for the warm case, during the first part of the forecasts (February–March), both the T42 and T106 models produce a HC anomaly distribution similar to the observations. Then, while the T42 anomalies decay quickly, in the T106 case the disturbance is sustained, and at the end of the forecast period the high-resolution model produces anomaly patterns closer to the observations.

4.2.2. Vertical structure of the ocean temperature in the equatorial Pacific. The HC anomalies shown in Figs. 6–11 are a measure of the integrated vertical temperature anomalies from the sea surface to the depth of 300 m. More detailed information about the actual vertical thermal structure that characterizes the development of the ENSO events can be gained by looking at the vertical section of the oceanic temperature in the equatorial Pacific.

Figure 12 shows the El Niño composites of the temperature anomaly in the upper 350 m of the equatorial Pacific (averaged between 2.5°N and 2.5°S). In the analysis (left column), during February and March, a large positive anomaly extends from the central-western Pacific to South America. The maximum is centred approximately at the depth of the thermocline. During the following months, the maximum of the positive anomaly moves to the east and closer to the sea surface. In the meantime, a large negative anomaly is developing in the western part of the basin.

In the models (middle and right columns), the positive anomaly of temperature produced during the first months of the forecasts is similar to the analysis results. However, consistent with the HC anomaly forecast shown in Fig. 11, with the T42 model the initial perturbation of the equatorial Pacific temperature is rapidly dissipated whereas, with the high-resolution atmosphere, the thermal perturbation is sustained, and its evolution is consistent with the observations. In particular, it is worth noting the appearence and the development of the negative anomaly in the western Pacific, in good agreement with the results obtained from the ocean analysis.

The composites of upper ocean thermal anomalies obtained from La Niña conditions (not shown) lead to results similar to the El Niño case (but the anomalies have the opposite sign). In February and March, a large negative temperature anomaly characterizes the upper part of the basin, extending from the central-western Pacific to the western coast of South America. The maximum is found at the depth of the thermocline and, in the analysis, tends to reinforce during the following months. As found for the forecasts of the warm ENSO phase, in the T42 case the amplitude of the anomaly decreases rapidly whereas, with the T106 model, the coupled system appears to be able to sustain the initial temperature perturbation, producing forecast anomalies whose evolution is close to the observations.

4.2.3. SST and near-surface zonal wind. The results presented so far seem to suggest an improvement of the ENSO forecasts obtained increasing the horizontal resolution of the atmospheric component of the model. This improvement might be due to a number of factors, such as, for example, a more accurate representation of orography, or the changes in the tuning parameters needed to run an atmospheric GCM at higher resolution. On

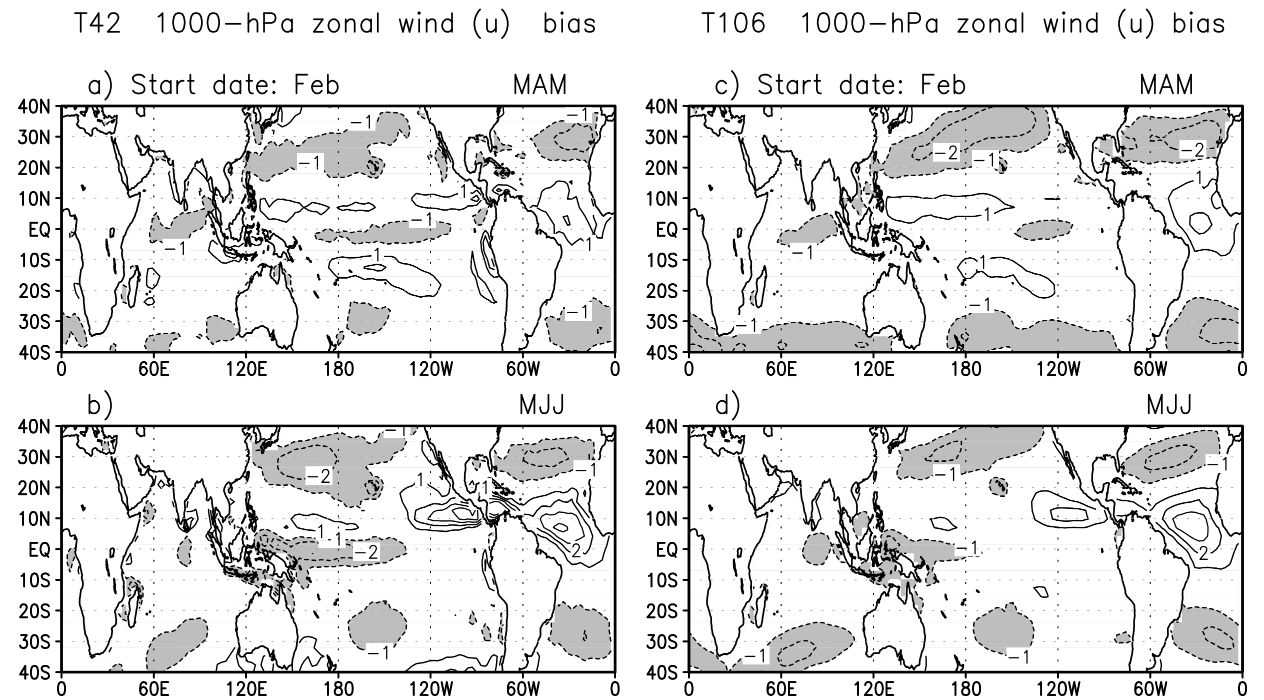

Fig 10. Model systematic error of the 1000-hPa zonal wind as obtained from T42 (left panels) and T106 (right panels) versions of the model. As for the SST, the error is defined as the difference between the climatology obtained from the forecast ensembles and the climatology obtained from the ERA-40 for the period 1982–1991/1996–2000. (a), (b) The 2–4 month (March–May) and 4–6 month (May–July) averages of the 1000-hPa zonal wind systematic error obtained from the T42 forecasts with start date 1 February. (c), (d) The 2–4 month (March–May) and 4–6 month (May–July) averages of the 1000-hPa zonal wind systematic error obtained from the T106 forecasts with start date 1 February. Contour is 1 m s^{-1}. Shaded patterns indicate negative anomalies with amplitude larger than 1 m s^{-1}.

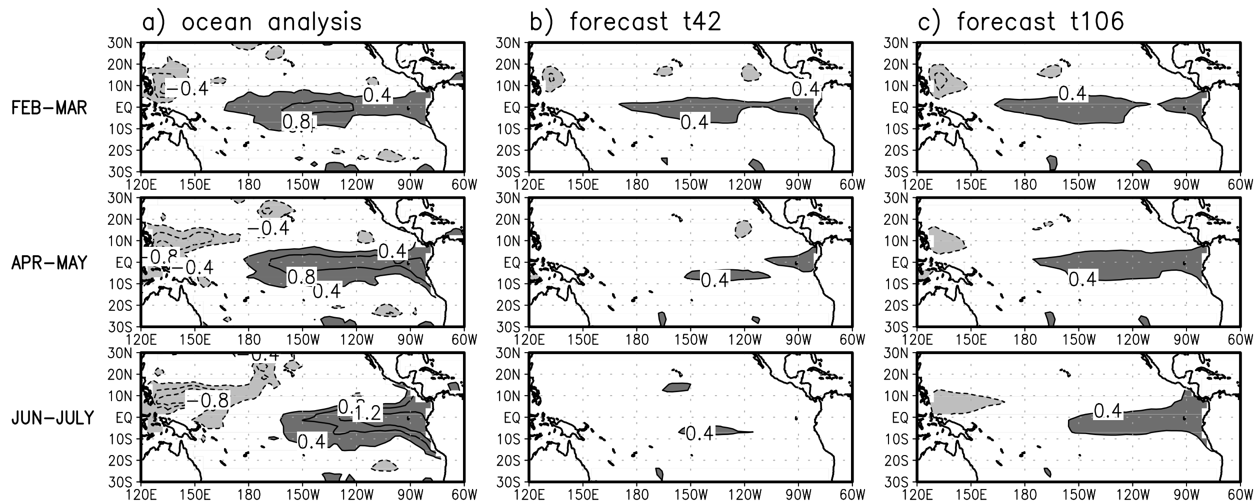

Fig 11. Composites of the HC anomaly in the tropical Pacific during the developing phase of warm ENSO (El Niño) episodes. The composite patterns depict the evolution of the HC anomalies for the period February–July, by averaging over the years 1982, 1987 and 1997. Left panels, ocean analysis; middle panels, T42 forecasts; right panels, T106 forecasts. Contour interval is 0.4 × 10^9 J m^{-2}. Dashed contour and light shaded patterns correspond to negative values; solid contour and dark shaded patterns correspond to positive values.

the other hand, the observed improvement might be explained by a better representation of the coupled air–sea processes yielded by the high-resolution atmospheric model. Specifically, in the equatorial region, the horizontal grid of the atmospheric model at T106 resolution is much closer to the ocean grid than at T42 resolution. Therefore, the SST distribution 'seen' by the T106 atmospheric model is significantly closer to the distribution actually produced by the ocean model than the SST patterns 'seen' by

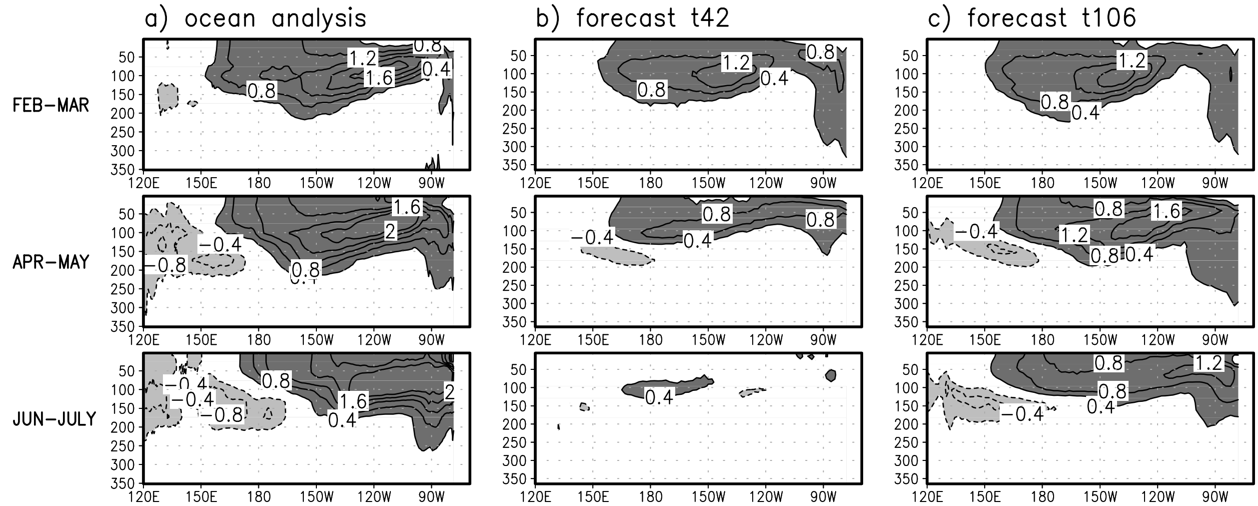

Fig 12. Composites of the temperature anomaly in the upper 350 m of the equatorial Pacific (average between 2.5°N and 2.5°S), during the developing (February–July) phase of warm ENSO events. As in Fig. 10, the evolution of the anomalies is depicted by composting the oceanic temperature anomaly over the year 1982, 1987 and 1997. Left panels, ocean analysis; middle panels, T42 forecasts; right panels, T106 forecasts. Contour interval is 0.4°C. Dashed contour and light shaded patterns correspond to negative values; solid contour and dark shaded patterns correspond to positive values.

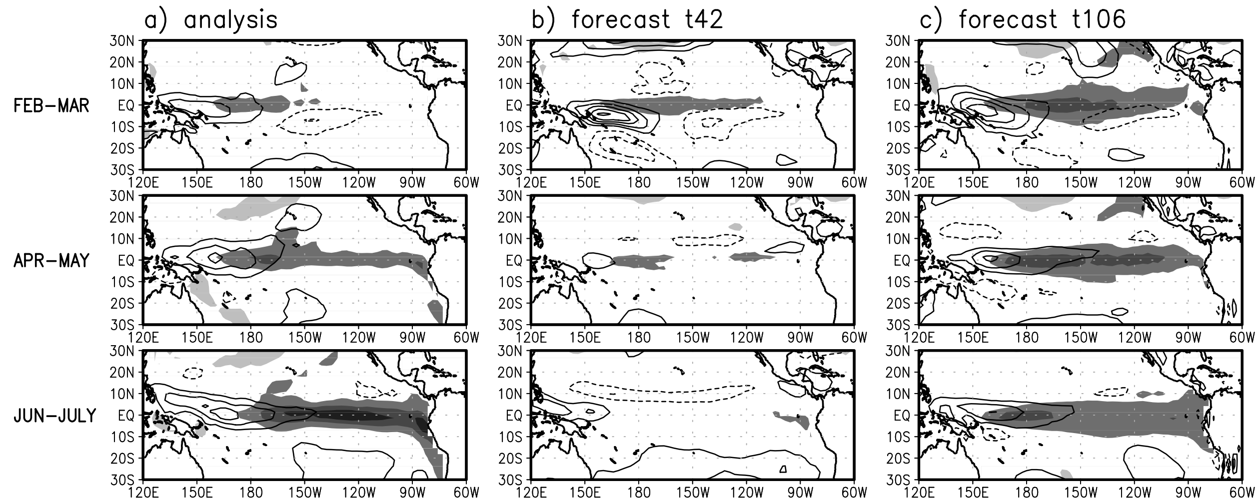

Fig 13. Composites of the SST (shaded patterns) and 1000-hPa zonal wind (contour patterns) anomaly in the tropical Pacific during the developing period (February–July) of El Niño events. The composites are obtained by averaging the anomalies over the years 1982, 1987 and 1997. Left column panels, ERA-40 results; middle column panels, T42 forecasts; right column panels, T106 forecasts. The SST contour interval is 0.5°C. Light (dark) shaded patterns correspond to negative (positive) values. Zonal wind contour interval is 1 m s^{-1}. Dashed (solid) contour corresponds to negative (positive) values.

the T42 atmosphere. In the latter case, the oceanic field is passed to the atmosphere after an interpolation to a much coarser grid, producing a smoothing and, possibly, a degradation of the SST gradients.

In the tropics, the surface winds that the atmospheric model produces are, to a great extent, a response to the SST distribution. Thus, the surface winds produced by the T106 version of the atmospheric model are more coherently related with the SST patterns actually produced by the oceanic model than the winds obtained with the T42 model.

In most simple ENSO models, the response of the atmospheric surface winds to the SST anomalies can be modulated by means of a parameter called 'coupling strength', which has been proved to play a key role in the ENSO mechanism (Zebiak and Cane, 1987; Neelin et al., 1998; Fedorov and Philander, 2000). In complex CGCMs it is difficult to identify a tunable parameter for the coupling strength. However, some insight can be gained by looking at the low-level wind anomaly.

Figure 13 shows the El Niño composites of SST (shaded patterns) and 1000-hPa zonal wind (contour patterns) anomalies, during the developing phase of the oscillation (February–July). In the reanalyses (left column), a positive wind anomaly is located over the western Pacific warm pool. The near-surface wind anomaly is accompanied by a positive SST anomaly, which, at the beginning of the examined period, is centred across the date line. Then, during the following months, the SST signal amplifies and extends across the equatorial Pacific from the date line to South America, whereas the wind anomaly elongates across the date line to the central equatorial Pacific.

In the T42 case (middle column), during the first forecast months (February and March), a positive zonal wind anomaly extends from the Maritime Continent to the date line. Consistent with the analysis, a positive anomaly of SST is found in the equatorial central Pacific, to the east of the westerly anomaly. However, similar to the results shown and discussed above, these wind and SST anomalies decrease very quickly, and during the following months of the forecast no other significant and coherent structures are found over the equatorial Pacific.

With the T106 model (Fig. 13, right column), the SST and surface wind anomalies persist throughout the forecast. Consistent with the ERA-40 results, the anomalous westerlies, initially confined into the western Pacific, cross the date line and elongate across the central equatorial Pacific during the second part of the forecast period. At the same time, the positive SST anomaly increases in the eastern part of the basin.

These results, along with those shown in Figs. 11 and 12, indicate that in the T106 model the wind anomalies sustain the thermal oceanic anomalies, which, in turn, feed back on the atmospheric circulation. This wind–oceanic temperature anomaly feedback seems to be less effective in the T42 model, as the rapid decay of the forecast anomalies seem to suggests.

In the composites obtained for La Niña forecasts (not shown), the anomaly patterns and their evolution are similar to the results found for the El Niño case, but with the opposite sign. Throughout the period February–July, a persistent near-surface easterly anomaly is observed over the equatorial western Pacific. In February and March, a concomitant negative anomaly of SST is observed in the equatorial Pacific, across the date line. In the model, with both resolutions, the SST anomaly maximum is shifted to the east.

Also in this case, the forecasts produced with the high-resolution atmosphere appear to be closer to the observations. In fact, while in the T42 model the SST and wind perturbations tend to be rapidly suppressed, in the T106 forecast the amplitude of the disturbances increases and, at the end of the forecast, the anomaly patterns appear to be in good agreement with the observations.

In summary, the results shown in Figs. 6–13 actually seem to suggest that an increase of the atmospheric horizontal resolution of the model leads, in general, to an improvement of the ENSO forecasts. A first, simple quantitative assessment of this improvement can be given by computing the correlation and the RMSE between the anomaly patterns as predicted by the models and as found in the observations.

In Fig. 14, the upper panels show the anomaly correlation coefficients (ACCs) between observations and T106 model (ordinate) versus the anomaly correlation between observations and T42 model (abscissa). Similarly, the plots in the lower panels show the RMSE between observations and T106 forecasts (ordinate) versus the RMSE between observations and T42 model (abscissa). Both the spatial correlations and the RMSEs have been computed for the tropical Pacific region (26°S–26°N, 120°E–90°W).

For all of the considered fields (HC, SST and 1000-hPa zonal wind), both the correlation and the RMSE analysis indicate that the forecasts obtained with the T106 model are, in general, closer to the observations. The T106 correlation (RMSE) values in fact tend to be systematically higher (lower) than the values obtained with the T42 model. Interestingly, the forecast improvement becomes more evident for the month 4–6 average values (empty circles).

5. Summary and conclusions

In this paper, we have analysed the capability of a seasonal forecast system based on a CGCM to predict ENSO anomalies. In particular, we have assessed the impact that the horizontal resolution of the atmospheric component of the model has on the forecast of the developing phase of intense ENSO.

As a first step, we have performed an analysis of the forecasts produced by the model in its standard configuration (T42). The analysis has focused on the prediction of the SST anomalies in the tropical Pacific. The forecasts consist of an ensemble of nine experiments performed starting from four different dates (1 February, 1 May, 1 August and 1 November), for every year in the period 1973–2001. At each start date, the initial conditions have been perturbed to represent the uncertainty in the knowledge of the initial state. Starting from the nine perturbed initial conditions, the CGCM has been integrated for six months.

The initial conditions for the atmosphere and ocean components have been created from integrations of the atmosphere and ocean models in forced mode. The forcing used for the atmosphere is an observational SST data set (Rayner et al., 2000); whereas the oceanic model has been forced with the ERA-40 surface fluxes.

The strategy we used to produce the initial conditions is rather simple. More advanced procedures, such as those using data assimilation techniques, produce higher-quality initial conditions, having, in turn, a beneficial impact on the quality of the forecasts (e.g. Fischer, 2002).

Although, in some cases, the initialization procedure has proven to be rough, the results we have shown, together with the results obtained in other studies (e.g. Palmer et al., 2004; see also the DEMETER web site), indicate that the basic skill of our model forecasts is reasonably good. In other words, the ENSO

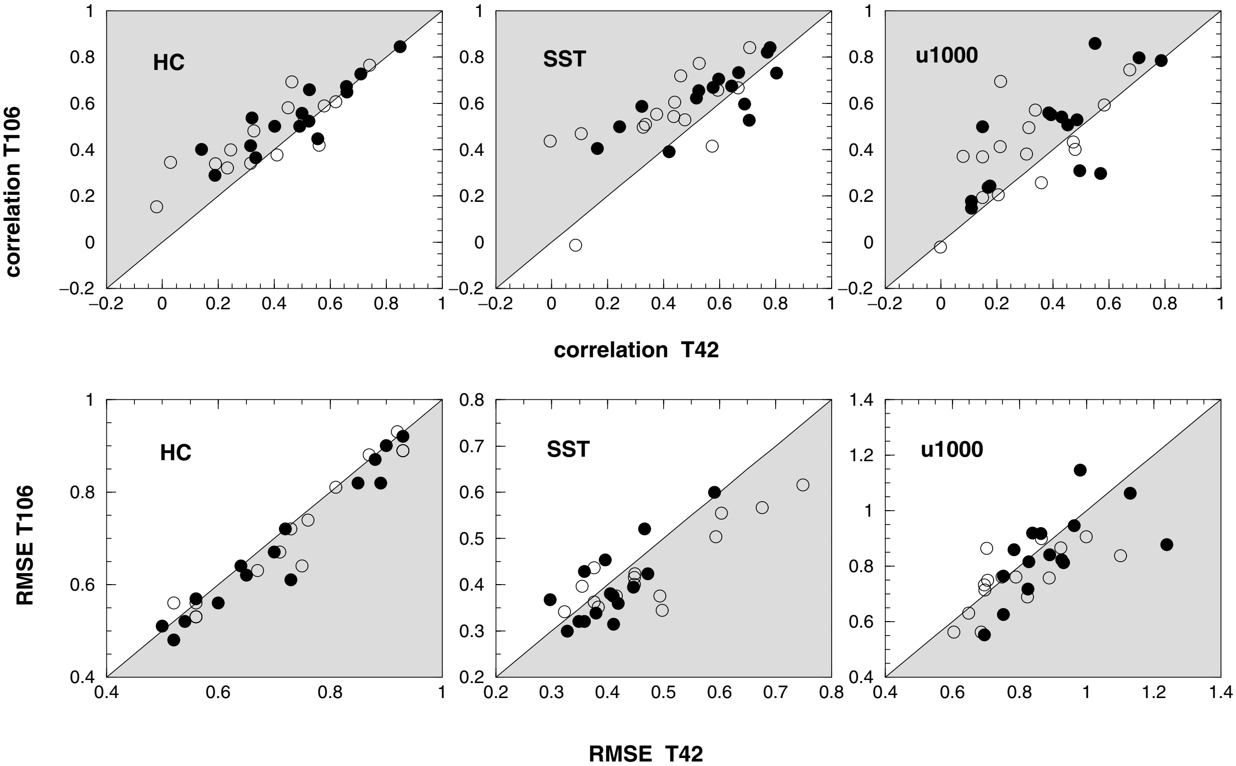

Fig 14. Upper panels: ACCs between observations and T106 model (ordinate) versus anomaly correlation between observations and T42 model (abscissa). The spatial correlations have been computed for HC (left panel), SST (middle panel) and 1000-hPa zonal wind (right panel) over the tropical Pacific (26°S–26°N, 120°E–90°W). Each point in the plot has as ordinate value the correlation between the observed and the T106 forecast anomaly, whereas the value along the abscissa is the correlation between the observed and the T42 forecast anomaly. The grey shaded portion of the plot indicates the values for which the T106 forecasts are closer to the observations than the T42 results. The filled circles are the results obtained from the month 2–4 averages, whereas the empty circles are the results obtained from the month 4–6 averages. Lower panels: as in the upper panels, but for the RMSE.

forecast skill of the system described here is comparable to the skill of other forecast systems based on CGCMs.

In particular, the model forecasts exhibit some skill in predicting the distribution of the SSTAs in the tropical Pacific. However, it has been shown that the predictions seriously underestimate the amplitude of the anomalies during the developing phase of strong ENSO events. It is noteworthy that the forecast errors are more pronounced for El Niño cases, whereas the amplitude of the predicted La Niña anomalies appears to be slightly closer to the observations.

The tendency to simulate weak ENSO anomalies is a feature common to many CGCMs (e.g. AchutaRao and Sperber, 2002). Also, the coupled model we used to produce the forecasts, the so-called SINTEX model, has the tendency to underestimate the amplitude of the ENSO SSTAs (Gualdi et al., 2003a; Guilyardi et al., 2003).

Beside the errors in the initial conditions, the model systematic errors are another important cause for the degradation of the forecasts. Schneider et al. (2003) have shown that both the model mean bias and higher-order statistics errors may induce severe errors in the forecasts. Results shown in Gualdi et al. (2003a) and Guilyardi et al. (2004) suggest that the model ENSO variability is significantly improved when the horizontal resolution of the atmospheric component of the model is increased.

In agreement with these studies, in this paper it has been shown that the increased horizontal resolution of the atmospheric model has a substantial impact on the forecasts of the growing phase of intense ENSO. More specifically, the prediction of both thermal anomalies in the ocean and surface wind anomalies in the tropical Pacific region appears to be improved when the atmospheric resolution is increased.

The results shown in this paper clearly indicate that the T42 version of the model appears to be inadequate to sustain the growth of the coupled disturbance during the developing phase of the strong ENSO events. In this case, in fact, the initial perturbation of the coupled system decays and the anomalies in the tropical Pacific vanish rather rapidly. On the other hand, when the high-resolution atmosphere is used, the coupled system appears to be able to sustain the coupled instability, which amplifies in a way similar to the observations.

The improvement of the results obtained with the increased atmospheric resolution is evident both for El Niño and La Niña forecasts. There are different possible factors that might lead to this improvement, which include, for example, a more accurate representation of orography and changes in the tuning parameters needed when the resolution of the atmosphere is increased. However, we think that a plausible explanation might be related to the fact that the resolution of the T106 grid is much closer to the oceanic grid resolution than the T42 grid. This is especially true in the equatorial region, which in turn is particularly important for the ENSO dynamics.

An atmosphere grid resolution closer to the ocean grid resolution implies a better atmospheric representation of the SST distribution. On the other hand, the surface winds are mainly driven by the SST distribution. Thus, the surface winds produced by the T106 model are more coherently related with the SST patterns actually produced by the oceanic model than the winds obtained with the T42 version of the model. The latter, in fact, are the response to an SST field that has been seriously degraded by the interpolation from a relatively high-resolution grid to a coarse one. Because the surface winds, in turn, play a major role in forcing the underlying ocean, a more coherent wind response to an anomalous oceanic state means a more coherent coupling between the ocean and the atmosphere.

In conclusion, with this paper we have shown that predictions of the growing phase of strong El Niño events are substantially improved when a high-resolution atmospheric component is used. The actual extent to which this improvement comes from a better capture of the details of the modelled SST or is due to atmosphere-only processes is still unclear and needs further investigations.

6. Acknowledgments

The authors are indebted to Dr A. Cherchi and Mrs L. Amato for technical support. They are also grateful to Dr S. Masina and Mr P. Di Pietro for providing the ocean analysis used in the study. Finally, they wish to thank two anonymous reviewers for their useful remarks and constructive criticisms. This work has been supported by the EU project DEMETER, contract EVK2-1999-00197.

References

AchutaRao, K. and Sperber, K. R. 2002. Simulation of the El Niño Southern Oscillation: results from the coupled model intercomparison project. *Climate Dyn.* **29**, 191–209.

Corti, S., Gualdi, S. and Navarra, A. 2003. Analysis of the mid-latitude weather regimes in the 200-yr control integration of the SINTEX model. *Ann. Geophys.* **46**, 27–37.

Davey, M., Huddleston, M., Sperber, K., Braconnot, P., Bryan, F. and co-authors. 2001. Stoic: a study of coupled model climatology and variability in tropical ocean regions. *Climate Dyn.* **18**, 403–420.

Doblas-Reyes, F. J., Hagedorn, R. and Palmer, T. N. 2005. The rationale behind the success of multi-model ensembles in seasonal forecasting – II. Calibration and combination. *Tellus* **57A**, 234–252.

Fedorov, A. and Philander, S. G. H. 2000. Is El Niño changing? *Science* **288**, 1997–2002.

Fischer, M. 2002. ENSO predictions with coupled ocean–atmosphere models. In: *Ocean Forecasting* (eds N. Pinardi and J. Woods). Springer-Verlag, Berlin, pp. 307–338.

Gualdi, S., Navarra, A., Guilyardi, E. and Delecluse, P. 2003a. The SINTEX coupled GCM. The tropical Indo-Pacific region. *Ann. Geophys.* **46**, 1–26.

Gualdi, S., Guilyardi, E., Navarra, A., Masina, S. and Delecluse, P. 2003b. The interannual variability in the tropical Indian Ocean as simulated by a CGCM. *Climate Dyn.* **20**, 567–582.

Guilyardi, E., Delecluse, P., Gualdi, S. and Navarra, A. 2003. Mechanisms for ENSO phase change in a coupled GCM. *J. Climate* **16**, 1141–1158.

Guilyardi, E., Gualdi, S., Slingo, J., Navarra, A., Delecluse, P. and co-authors. 2004. Representing El Niño in coupled ocean–atmosphere GCMs: the dominant role of atmospheric component. *J. Climate* **17**, 4623–4629.

Hagedorn, R., Doblas-Reyes, F. J. and Palmer, T. N. 2005. The rationale behind the success of multi-model ensembles in seasonal forecasting – I. Basic concept. *Tellus* **57A**, this issue.

Kanamitsu, M., Kumar, A., Juang, H.-M. H., Schemm, J.-K., Wang, W. and co-authors. 2002. NCEP dynamical seasonal forecast system 2000. *Bull. Am. Meteorol. Soc.* **83**, 1019–1037.

Latif, M., Anderson, D., Barnett, T., Cane, M., Kleeman, R. and co-authors. 1998. A review of the predictability and prediction of ENSO. *J. Geophys. Res.* **103**, 14 375–14 393.

Madec, G., Delecluse, P., Imbard, M. and Levy, C. 1998. OPA 8.1 ocean general circulation model reference manual. *Tech. Rep. LODYC/IPSL Note* **11**, 91 pp.

Masina, S., Pinardi, N. and Navarra, A. 2001. A global ocean temperature and altimeter data assimilation system for studies of climate variability. *Clim. Dyn.* **17**, 687–700.

Mason, S. J., Goddard, L., Graham, N. E., Yulaeva, E., Sun, L. and co-authors. 1999. The IRI seasonal climate prediction system and the 1997/98 El Niño event. *Bull. Am. Meteorol. Soc.* **80**, 1853–1873.

Neelin, D. J., Battisti, D. S., Hirst, A. C., Jin, F.-F., Wakata, Y. and co-authors. 1998. ENSO theory. *J. Geophys. Res.* **103**, 14 261–14 290.

Palmer, T. N., Alessandri, A., Andersen, U., Cantelaube, P., Davey, M. and co-authors. 2004. Development of a European Multi-model Ensemble System for Seasonal to Interannual Prediction (DEMETER). *Bull. Am. Meteorol. Soc.* **85**, 853–872.

Perigaud, C., Melin, F. and Cassou, C. 2000. ENSO simulated by intermediate coupled models and evaluated with observations over 1970–98. Part I: role of the off-equatorial variability. *J. Climate* **13**, 1605–1634.

Philander, S. G. H. 1990. *El Niño, La Niña and the Southern Oscillation*, Academic, San Diego, 293 pp.

Rayner, N. A., Parker, D. E., Frich, P., Horton, E. B., Folland, C. K. and co-authors. 2000. SST and sea-ice fields for ERA-40. *Proceedings of the 2nd WCRP International Conference on Reanalyses, Reading,* UK, August 1999, WCRP-109, WMO/TD-No. 985, pp. 18–21.

Reynolds, R. W. and Smith, T. M. 1994. Improved global sea surface temperature analyses using optimal interpolation. *J. Climate* **7**, 929–948.

Roeckner, E., Arpe, K., Bengtsson, L., Cristoph, M., Claussen, M. and co-authors. 1996. The atmospheric general circulation model ECHAM-4: model description and simulation of present-day climate. *Max-Planck-Institut für Meteorologie Rep.* **218**, 94 pp.

Ropelewski, C. F. and Halpert, M. S. 1987. Global and regional scale precipitation patterns associated with El Niño/Southern Oscillation. *Mon. Wea. Rev.* **115**, 1606–1626.

Schneider, E. K., DeWitt, D. G., Rosati, A., Kirtman, B. P., Ji, L. and co-authors. 2003. Retrospective ENSO forecasts: sensitivity to atmospheric model and ocean resolution. *Mon. Wea. Rev.* **131**, 3038–3060

Stern, W. and Miyakoda, K. 1995. Feasibility of seasonal forecasts inferred from multiple GCM simulations. *J. Climate* **8**, 1071–1085.

Valcke, S., Terray, L. and Piacentini, A. 2000. The OASIS coupler user guide version 2.4. Tech. Rep. TR/CMGC/00-10, CERFACS, 88 pp.

Webster, P. J. 1995. The annual cycle of and the predictability of the tropical coupled ocean–atmosphere system. *Meteorol. Atmos. Phys.* **56**, 33–55.

Xie, P. and Arkin, P. A. 1997. Global precipitation: A 17-yr monthly analysis based on gauge observations, satellite estimates and numerical model outputs. *Bull. Am. Meteorol. Soc.* **78**, 2539–2558.

Zebiak, S. E. and Cane, M. A. 1987. A model of El Niño Southern Oscillation. *Mon. Wea. Rev.* **115**, 2262–2278.